Chapter-III

Rare Earth (Gd^{3+}) doped Lanthanum Chromite Based ($LaCrO_3$) Anode System

Paper published from this chapter

***1.Pravin Kumar**, Rajesh Kumar Singh, A.S.K. Sinha, Prabhakar Singh, Effect of isovalent ion substitution on electrical and dielectric properties of LaCrO3, Journal of Alloys and Compounds 576, 154–160 (2013).*

***2. Pravin Kumar**, Rajesh Kumar Singh and Prabhakar Singh, Structural and Electrical Characterizations of Lanthanum Chromite: Effect of Synthesis Routes, Trans. Ind. Ceram. Soc., vol. 71, no. 4, pp. 239-242 (2013).*

3.1 Overview

The recent development of low-cost materials having high durability and fuel flexibility at cell operating temperature is one of the prominent challenges. The prime objective for the commercialization of SOFCs is to reduce the operating temperature of operation using new cost-effective potential anodes, which exhibits high electronic conductivity in the intermediate or low temperature range [Wachsman and Lee (2011), Tarancón (2009) and Huang et al. (2012)]. Among the components of SOFC, anode plays a key role in the successful operation of the device. Besides this, anodes with improved electronic conductivity at low or moderate temperatures for SOFC along with the co-firing process of the component materials (i.e., air electrode, electrolyte, and fuel electrode) at low sintering temperature (1000-1300 °C), are highly desirable [Huang et al. (2012)]. Therefore, in investigation of low cost and widely stable materials, perovskite structured lanthanum chromite has also been proposed as a potential anode for SOFCs. Its electronic conductivity is sufficient for the use as an anode only at higher temperatures (800-1000 °C) [Badwal (1992) and Kim (1989)]. This material offers not only high electronic conductivity but also low ionic conductivity. $LaCrO_3$ with suitable doping has been proposed as promising nickel-free anode material for solid oxide fuel cells [Boukamp et al. (2003), Tao et al. (2003), Sfier et al. (2003) and Kolotygin et al. (2013)]. Among various existing anode materials, nickel/YSZ and Fe/Co lanthanum chromite perovskite, doped with alkaline earth substituent, has high p-type conductivity and are found be stable over vide range of oxygen partial pressure [Boukamp et a. (2003), Kolotygin et al. (2013) and Dong et al. (2012), Zhu et al.(2012)]. Lanthanum chromite ($LaCrO_3$) is a perovskite type structure having general formula ABO_3. It is a p-type electronic conductor under the oxidizing condition and found to show orthorhombic structure with space group *Pnma* at the room temperature [Mukherjee et al. (2012) and Correa et al. (2008)]. The phase transition of $LaCrO_3$ from orthorhombic to a rhombohedral and rhombohedral to cubic occurs at around 260°C and 1600°C, respectively [Oikawa et al. (2000)]. Among various perovskite materials, mixed electronic/ionic conductivity of $LaCrO_3$ plays an important role in enhancing SOFC performance [Suthirakun, et al. (2012)]. Electrical properties of this system have been studied extensively in pure and doped forms. The Sr^{2+} doped lanthanum chromite, $La_{1-x}Sr_xCrO_3$, represented thermally activated temperature dependence of electrical conductivity over a wide temperature range [Karim et al. (1979)].

This chromite based system was found to exhbit temperature dependent carrier mobility rather than carrier concentration. The presence of higher valence state of chromium ions (Cr^{6+}) affected the electrical conductivity of $La_{1-x}Sr_xCrO_3$ [Liu et al. (2012)]. Ca doped $LaCrO_3$ was found to show thermally activated small hole-polaron hopping conduction [Mukherjee et al.(2012)]. Jiang et al. [2008] reported that for $La_{1-x}M_xCrO_3$ system (with M = Mg, Ca, Ba, Sr), Ca and Sr doped compositions show highest conductivity. The electrical conductivity of $LaCrO_3$ increases by doping of Ca and Ba, however, the Ba doped system shows maximum conductivity [Ong et al.(2007)]. Zhang et al. [2002] have measured electrical conductivity of mixed doped $La_{0.9}Ca_{0.1}Cr_{0.5}Ni0_{.5}O_3$ system and showed a phase transition at 465 K. Divalent cations (like Ca, Sr, Ba etc) at trivalent site (La-site) in $LaCrO_3$ creates more holes in the valence band, which reduces the energy band gap leading to an increase in conductivity of this system [Nithya et al. (2012)]. The heterovalent substitution in the lanthanum chromite system has also been studied by various research groups. Doping of rare earth (Sm^{3+}) on lanthanum site, forming an isovalent system, has been studied by Shaikh and Rashad et al. [2010]. Dong et al. [2012] reported that rare earth cerium (Ce^{3+}) doped $LaCrO_3$ has been proposed as potential anode candidate for SOFC.

In present chapter, we have reported the structural and electrical properties of rare earth (Gd^{3+}) doped lanthanum chromite, $La_{1-x}Gd_xCrO_3$ (x=0.00, 0.01, 0.05, 0.10, 0.15, 0.20); system has been synthesized via facile auto-combustion route. The ionic size of dopant ion, Gd^{3+} (0.94 Å) is smaller than the ionic size of the host ion, La^{3+} (1.061), so it was considered worthful to understand the effect of size and concentration of dopant ions on the structural and electrical properties of $LaCrO_3$ system.

3.2 Experimental and characterization techniques

A series of a few compositions of rare earth (Gd^{3+}) doped lanthanum chromite; $La_{1-x}Gd_xCrO_3$ ($0.00 \leq x \leq 0.20$) was synthesized via auto-combustion synthesis route. The auto-combustion route is relatively simple, fast and cost effective method. The investigated system was synthesized by using stoichiometric amount of La_2O_3, Cr_2O_3 and Gd_2O_3 as starting materials of Alfa-Aesar having purity more than 99.9 %. A detailed synthesis and characterization procedure have already been discussed in chapter-II. Samples were characterized employing XRD, SEM, FTIR, XPS and Electrochemical impedance techniques. The phase investigation, structure, and lattice parameters of the samples were determined

using X-ray powder diffraction (Rigaku Miniflex II desktop) with Cu-Kα radiation (λ ≈ 1.54 Å) at room temperature. Sintered pellets were polished and coated with a high temperature Ag-paint on both sides to characterize the conductance by Wayne Kerr (6500 P Series) LCR meter in entire frequency range 20 Hz to 1 MHz and temperature range 40 °C to 520 °C using two-probe method. The grain and grainboundary morphology were studied using scanning electron microscopy (LEO-1455). The FT-IR spectra have been used in the 4000–400 cm^{-1} range with a Shimadzu spectrometer using the KBr dilution technique. The density of each composition has been measured by Archimedes Principle employing Mettler-Toledo density measurement kit attached to weighing balance. XPS spectra of a few compositions were measured on a KRATOS (Amicus model) high performance analytical instrument using Mg Kα (X-ray source, hν = 1253.6 eV) target under 1.0 x 10^{-6} Pa pressure.

3.3. Results and Discussion

3.3.1. XRD Analysis

Phase confirmation and structural parameters of the powders materials of various compositions were investigated using XRD data. The peaks in XRD data, of all doped and undoped samples, show high intensity indicating high crystalline nature of the samples is shown in Fig.3.1. The single phase formation of $LaCrO_3$ was confirmed by absence of characteristic lines of constituent oxides or any other phases. Figure.3.2 represents the Rietveld refinement of XRD data for all prepared samples. The peak reflections were modelled by using pseudo-voigt function and back ground has been described in terms of twelve coefficient polynomial. The R_{wp} (weighted-pattern factor) and S (goodness-of-fit) parameters were used as numerical criterion of quality of the fit to calculate to experimental diffraction data. The structural parameters of the powders were investigated by Rietveld analysis of XRD data applying *FullProf* software. Rietveld refinement of all samples of XRD data represented the orthorhombic structure with space group *Pnma* at room temperature. It is observed that in this sample, the increase in *a* value is compensated by decrease in *c* value so that the total volume remains almost constant. The percentage density of each composition was calculated from the experimental value and is tabulated in Table3.1. The density of investigated compositions resembles with the data published earlier (or better) [Jiang et al.

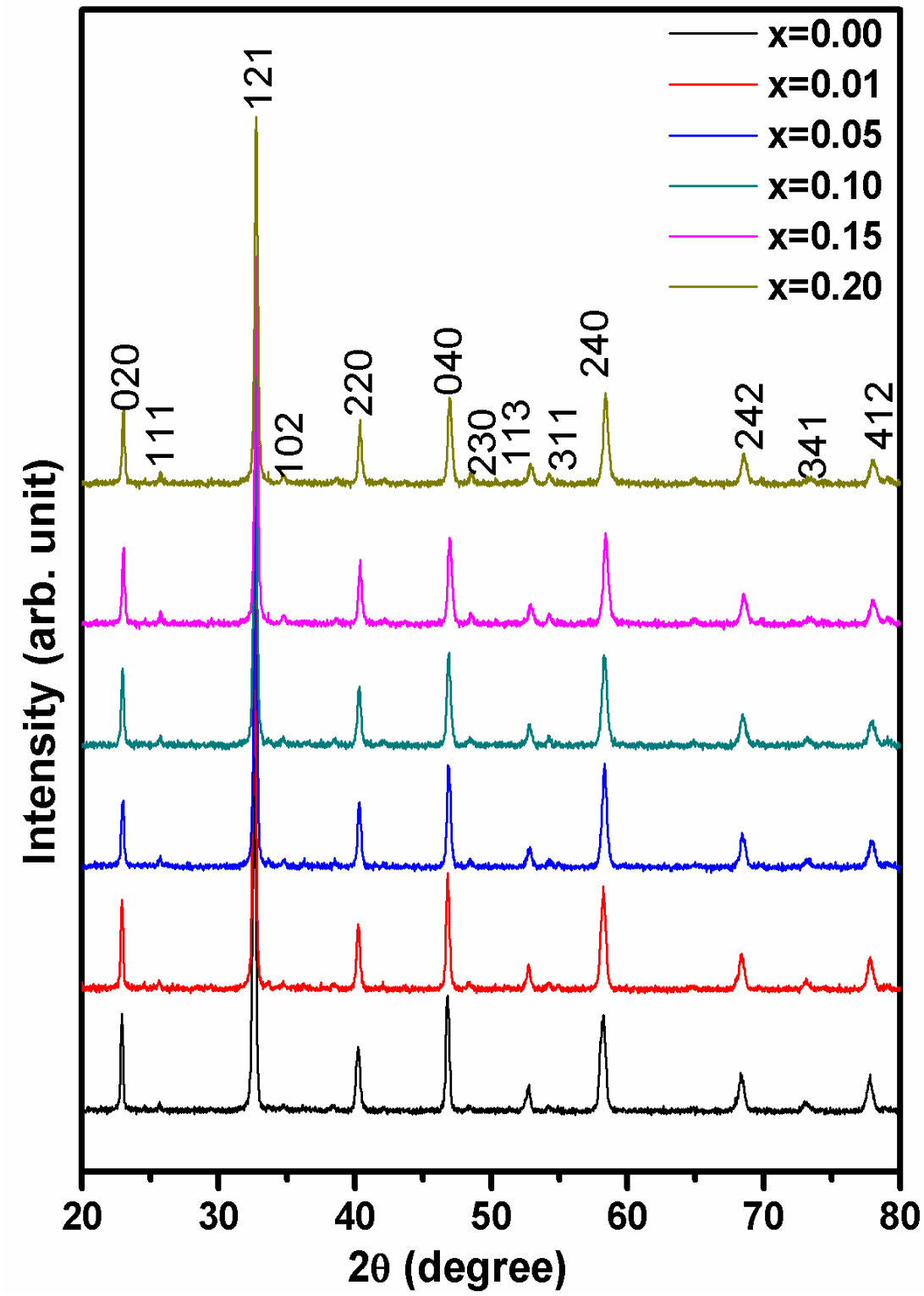

Fig.3.1 *The X-ray diffraction pattern of* $La_{1-x}Gd_xCrO_3$ *(0.00 ≤ x ≤0.20) system.*

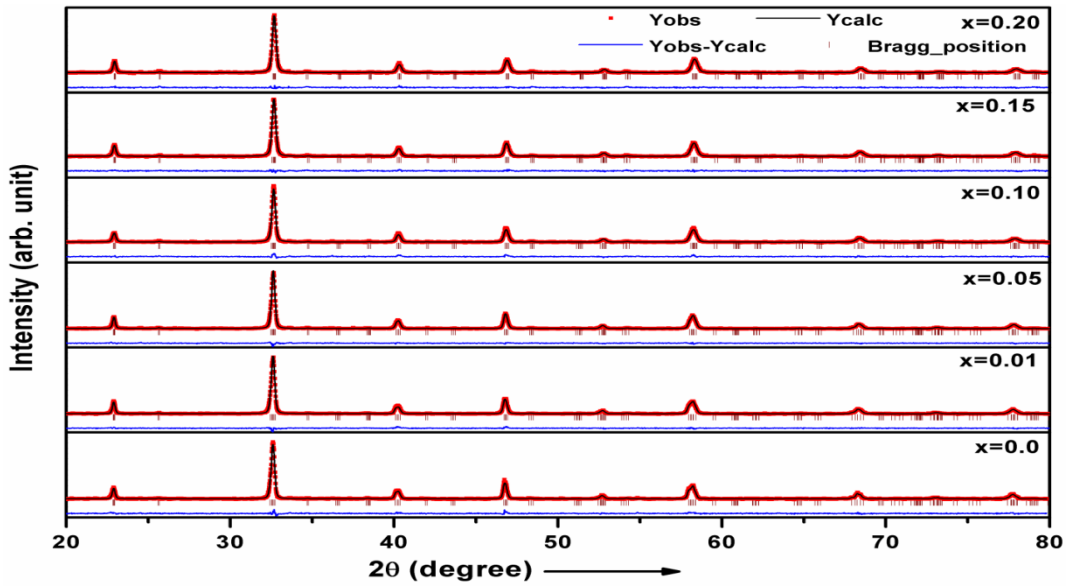

Fig. 3.2: Reitveld refinement of *X-Ray diffraction pattern of* $La_{1-x}Gd_xCrO_3$ *(0.00 ≤ x ≤0.20) system. Here Yobs, Ycal,Yobs-Ycal and Bragg_Position represent the experimental data, calculated data, the difference of experimental and calculated data and Bragg's positions, respectively.*

Table 3.1: *Various parameters obtained from Rietveld refinement analysis of the XRD data and the density measurements of* $La_{1-x}Gd_xCrO_3$ *(0.00 ≤ x ≤0.20) system.*

Sample $La_{1-x}Gd_xCrO_3$	Lattice parameters			Cell Volume $(Å)^3$	Crystallite Size (nm)	χ^2	Percent of theoretical density
	a (Å)	b (Å)	c (Å)				
x=0.00	5.4788	7.7596	5.5149	234.46	51	5.283	84.71
x=0.01	5.4776	7.7573	5.5142	234.30	97	3.088	84.39
x=0.05	5.4771	7.7538	5.5083	233.93	74	0.5751	83.81
x=0.10	5.4764	7.7465	5.5019	233.41	55	0.4544	82.96
x=0.15	5.4737	7.7443	5.4979	233.06	72	0.2576	82.93
x=0.20	5.4880	7.7453	5.4737	232.67	60	0.1978	82.60

[2008], Rahmauni et al. (2012)]. The average crystallite size of all prepared samples were calculated using Wiilliamson- Hall equation $\beta Cos\theta = K\lambda/t + 2\varepsilon Sin\theta$, *where* β (in radians) is

the full width at half maximum (FWHM) intensity of a Bragg reflection for XRD of all the peaks excluding the instrumental broadening, θ is a Bragg diffraction angle, K is Scherrer's constant, λ is wavelength of X-ray radiation and ε be the lattice strain. The crystallite size was calculated from the Williamson-Hall plot using MDI Jade software and is given in Table 3.1.

3.3.2 FTIR Study

The FT-IR spectrum for the composition $La_{0.99}Gd_{0.01}CrO_3$ is shown in Fig.3.3. The absorption bands at 449, 594, and 636 cm^{-1} are assigned to O-Cr-O, Cr-O, Cr-O stretching modes of vibrations, respectively and weak intensity absorbed peak at 920 cm^{-1} was assigned to the La-O stretching vibrations. Similar result has been reported by Sheikh et al. [2010] for this system.

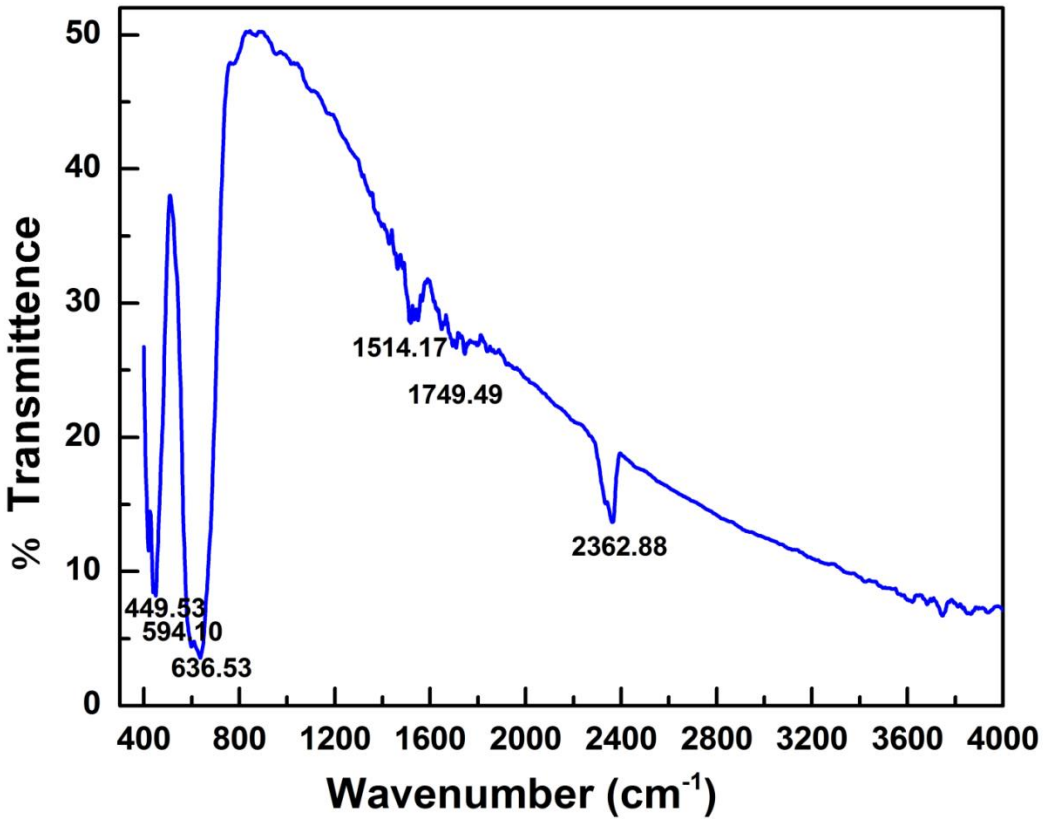

Fig. 3.3: *FTIR spectrum of $La_{0.99}Gd_{0.01}CrO_3$.*

The usual peaks appearing at 1650 cm^{-1} and 3600 cm^{-1} are assigned to the symmetric stretching and asymmetric stretching modes of vibrations, respectively which demonstrate that water molecules are adsorbed at the sample surface. No absorption peak corresponding to

Gd^{3+} associated bond is observed in the IR spectra of the investigated system. This is also a good agreement with formation of single phase solution in the system $La_{1-x}Gd_xCrO_3$.

3.3.3 SEM Study

SEM microstructure of all the compositions of $La_{1-x}Gd_xCrO_3$ synthesized using facile auto combustion is depicted in Fig3.4 (a)-(f). The microstructural result shows the spherical, oval and irregular morphology. The SEM images also show the formation of cluster and agglomeration of powder particles. The grain size of Gd^{3+} doped $LaCrO_3$ samples slightly reduces as compared to pure $LaCrO_3$. Figure.3.3 (a)-(f) indicates that the average grain size of $La_{1-x}Gd_xCrO_3$ system is found between 0.5 to 1.0 μm. The variation of microstructure of all compositions shows that the substitution of Gd^{3+} on La^{3+} of lanthanum chromite slightly affects the grain size. The relative grain sizes of microscopic particles first decreases and then gradually increases with increase in dopant concentrations.

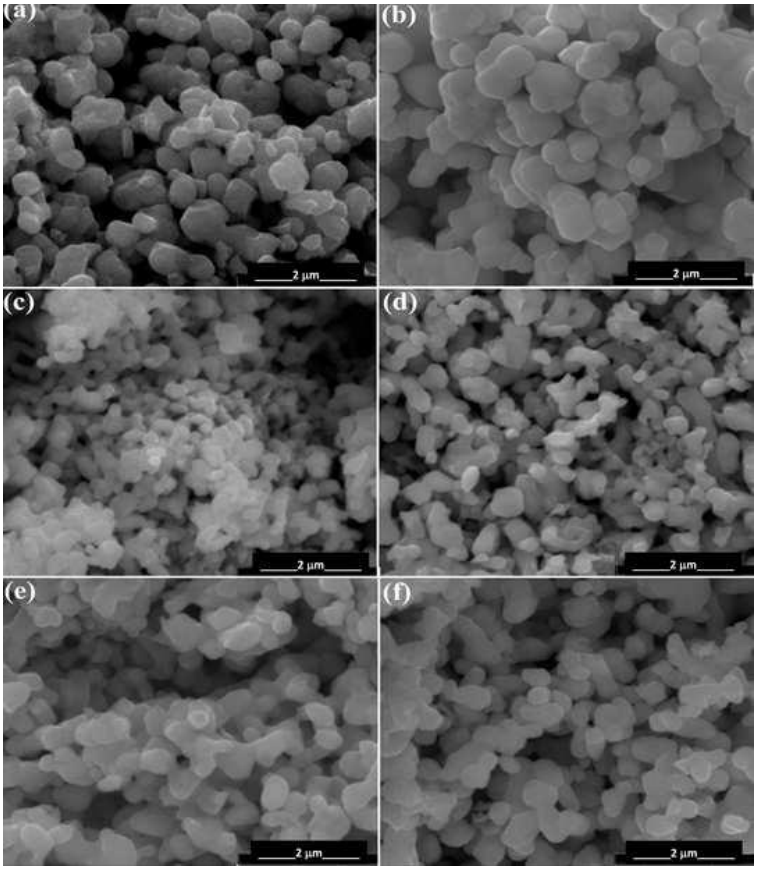

Fig. 3.4. *SEM micrograph of $La_{1-x}Gd_xCrO_3$ [**(a)** x= 0.00, **(b)** x= 0.01, **(c)** x= 0.05, **(d)** x= 0.10, **(e)** x= 0.15, and **(f)** x= 0.20] system.*

3.3.4 Electrical Conductivity

The real part of conductivity spectra of $La_{1-x}Gd_xCrO_3$ system is shown in Fig.3.5 (a)-(b) for x = 0.01 and 0.10 at a few temperatures. This figure clearly indicates a frequency independent conductivity in almost entire frequency range. Similar behaviour has been obtained for all other samples. Generally, any ceramic, glass or polymer materials display frequency independent conductivity (DC conductivity) followed by a dispersion regime (frequency dependent part i.e. AC conductivity) in their conductivity spectra. In present case, it seems that the dispersion regime will appear in further high frequencies. Nithya et al. [2012] have reported similar behaviour for $LaCr_{0.5}Cu_{0.5}O_3$ and $LaCr_{0.5}Fe_{0.5}O_3$ system in their conductivity spectra.

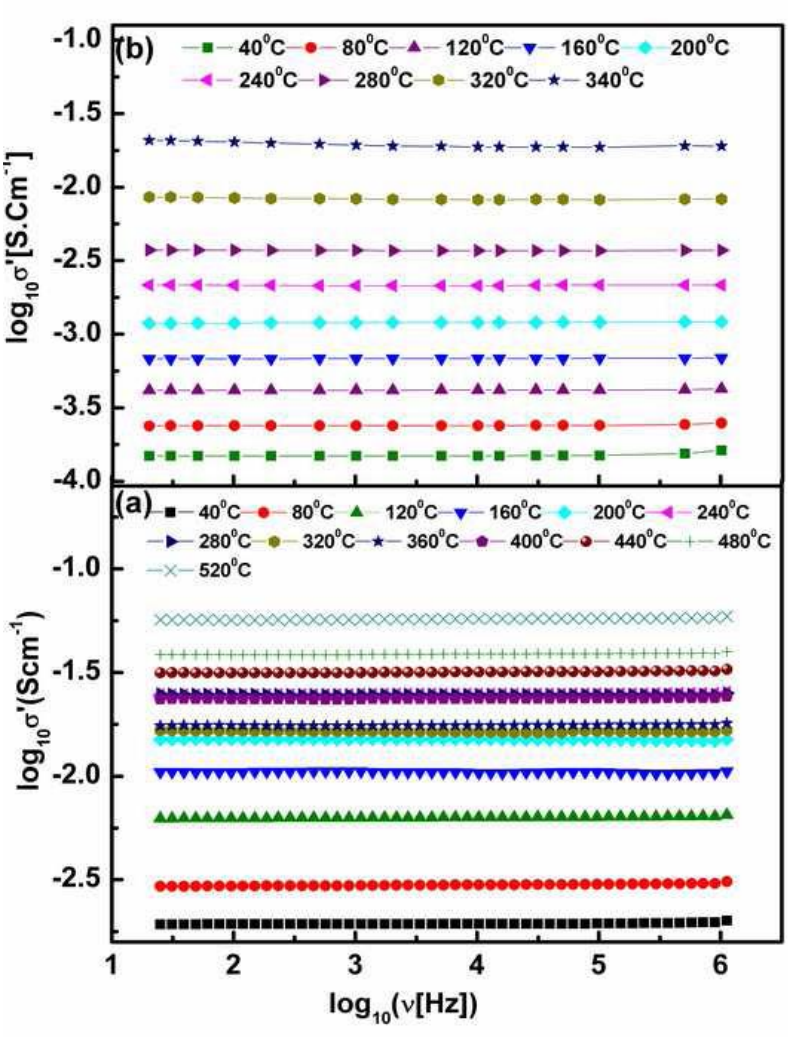

Fig. 3.5: *Representative conductivity spectra of $La_{1-x}Gd_xCrO_3$ for (a) x = 0.01 and (b) x = 0.10, at a few temperatures.*

These systems were found to exhibit dispersion in conductivity spectra after about ~1 MHz. Nevertheless, DC conductivity, σ_{DC}, can be evaluated at the measured temperatures by extrapolating the low frequency plateau of the conductivity spectra. The Arrhenius plot of the DC conductivity, obtained from the low frequency plateau, for all compositions is shown in Fig.3.6. The obtained DC conductivity values are superior to the value reported by Tripathi et al. [1982]. Some groups have reported DC conductivity value of pure lanthanum chromite higher than the value reported here [Jiang et al. [2008], Rahmauni et al. (2012)]. This may be due to the fact that in the present case DC conductivity are evaluated from the low frequency plateau of the conductivity spectra, which shows relatively low value due to electrode polarization dominating at low frequencies.

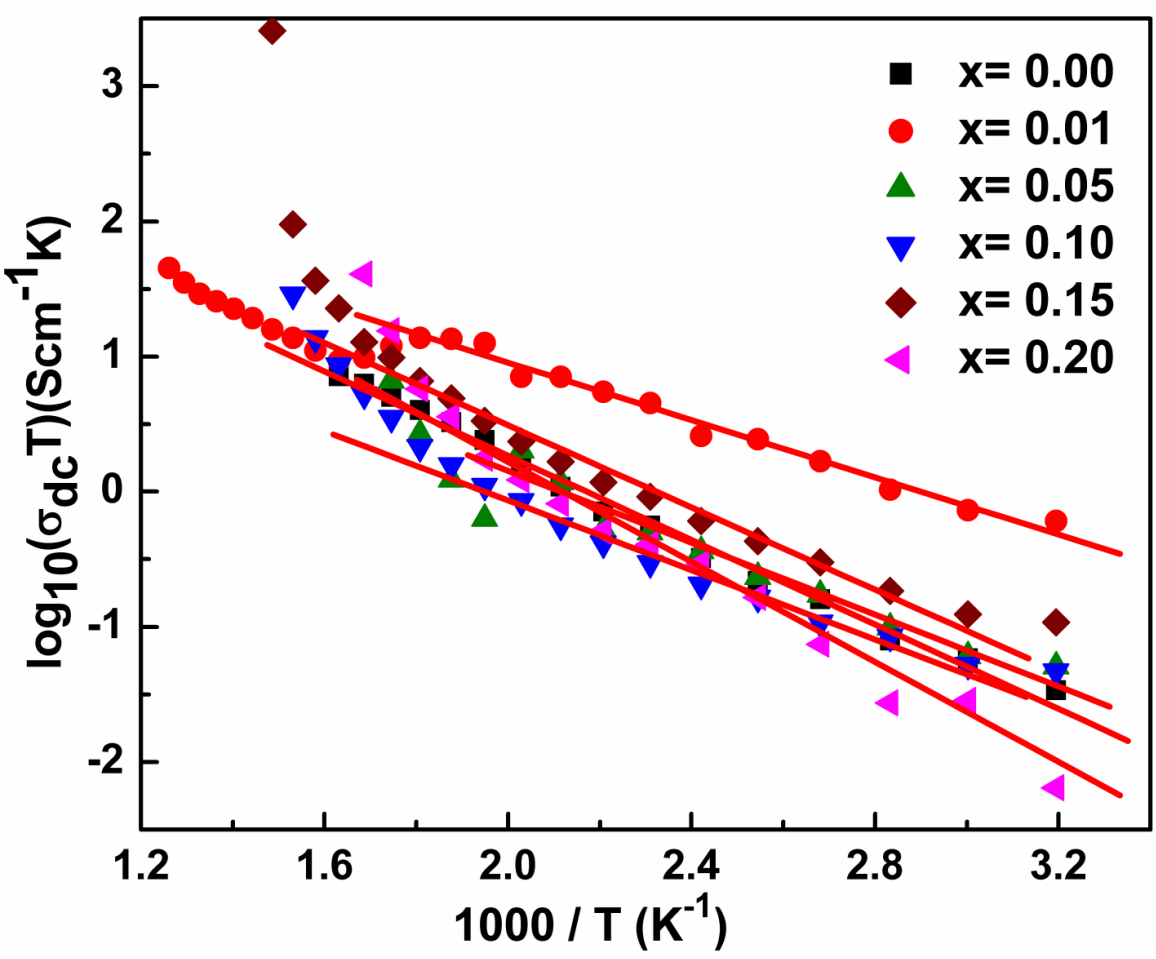

Fig.3.6: *Arrhenius representation of DC conductivity of $La_{1-x}Gd_xCrO_3$ ($0.00 \leq x \leq 0.20$). The symbols denote the experimental (calculated) data points and the solid lines represent the linear fit to the data points.*

This figure reveals that DC conductivity, for all compositions, follows linear behaviour at lower temperatures, however, a non linear behaviour is discerned for the compositions with x ≥ 0.10 above about 300 °C. For compositions with x ≥ 0.10 the DC conductivity is found to increase rapidly above 300 °C. The linear region represents that DC conductivity is thermally activated following the Arrhenius equation $\sigma_{DC}.T = \sigma_0 \cdot exp(E_a/kT)$, where, σ_0 is pre exponential factor, E_a be the activation energy for conduction, k is the Boltzmann constant and T is the absolute temperature. The activation energy for all compositions has been calculated from the slope of the linear region and is reported in Table.3.2.The compositional dependent DC conductivity at a few temperatures is shown in Fig.3.7. From this figure, it is clear that DC conductivity first increases up to x = 0.01 and then it shows decreasing trend up to x = 0.10 and thereafter again it shows an increasing trend of conductivity for the compositions x = 0.15 and 0.20. The temperature and compositional dependent electrical conduction behaviour of the $La_{1-x}Gd_xCrO_3$ system can be understood in the following way. Pure lanthanum chromite is a p-type conductor. [Webb et al. (1977), Rao et al. (1998)] and the doped $LaCrO_3$ have been reported to show a polaronic conduction [Tao et al. (2003)].

Table 3.2. *Activation energy for conduction for various compositions of $La_{1-x}Gd_xCrO_3$ ($0.00 \leq x \leq 0.20$) system.*

$La_{1-x}Gd_xCrO_3$	Temperature range	Activation Energy (eV)
X=0.00	40-340 ^{0}C	0.31
X=0.01	40-300 ^{0}C	0.21
X=0.05	40-220 ^{0}C	0.26
X=0.10	60-280 ^{0}C	0.25
X=0.15	60-320 ^{0}C	0.30
X=0.20	40-280 ^{0}C	0.39

In $LaCrO_3$, presence of a large number of Cr^{4+} centers due to native defects in this system has been reported [Rao et al. (1971)]. Moreover, the ^{151}Eu Mossbauer spectra measurement of isovalent Eu^{3+} doped $LaCrO_3$ shows the presence of Cr^{6+} ions in this system [Wei et al.

(1997)]. Due to presence of these higher valent cations, holes are generated as per the following defect reaction [Tripathi et al. (1982)].

$$\left.\begin{aligned} 3Cr^{3+} + 3h^{\cdot} &\rightarrow 3Cr^{4+} \\ Cr^{3+} + 3h^{\cdot} &\rightarrow Cr^{6+} \end{aligned}\right\} \quad (3.1)$$

The holes, generated from the above equation, along with the lattice interaction form small polarons.

In present $La_{1-x}Gd_xCrO_3$ system, for very low concentration of Gd^{3+} ($x \leq 0.01$), the isovalent dopant ions, Gd^{3+}, do not create any additional defect in the system, and the conductivity is due to the polarons generated from Eqn.3.1. Thus the conductivity of $La_{1-x}Gd_xCrO_3$ system increases till x = 0.01. However, when $x \geq 0.01$, the "size effect" plays an important role in the conduction process [Lee et al. (2001)]. In the case of isovalent substitution, an additional creation of oxygen vacancies due to considerable size difference between the constituent (host and dopant) ions has been reported [Shahi et al. (1980, 1981)]. In present case, the ionic radii of Gd^{3+} and La^{3+} ions are 0.94 Å and 1.061 Å, respectively. Consequently this size difference could encourage the generation of oxygen vacancies, which could be expressed using the Kroeger-Vink notation by

$$Gd_2O_3 \rightarrow 2Gd_{La}^{\times} + 3V_O^{\cdot\cdot} + 3O_i'' \quad (3.2)$$

These oxygen vacancies may lead to decrease in conductivity of $La_{1-x}Gd_xCrO_3$ system as concentration of dopant ion becomes larger than 0.01. Furthermore, Figure.3.6 indicates that the conductivity of the investigated system again starts to increase for the compositions with $x \geq 0.15$. Li et al. [1997] have reported that the amount of Cr^{6+} ions increases with increasing concentration of isovalent Eu^{3+} substituting isovalent La^{3+} ion in $LaCrO_3$ system. To confirm the presence of Cr^{6+} ions in the $La_{1-x}Gd_xCrO_3$ system, we measured XPS spectra of a few compositions of this system. The Cr-2p level spectra of $La_{1-x}Gd_xCrO_3$ system for x = 0.00, 0.01 and 0.20 are shown in Fig.3.8. Leiro et al. [1984] have measured XPS spectra of metallic chromium. They assigned a peak at about ~576 eV to Cr-$2p_{3/2}$ (Cr^{3+} state) and a peak at about ~582 eV to Cr-$2p_{1/2}$ (Cr^{6+} state). Similar results have been reported for other doped lanthanum chromite systems [Kobsiriphat et al. (2010), Li et al. (1997), Liu et al. 2001)]. From Figure.3.7, it is clear that the undoped $La_{1-x}Gd_xCrO_3$ system (for x = 0.00) depicts peak only

at about ~576 eV and no peak at ~582 eV showing the presence of Cr^{3+} ions and absence of Cr^{6+} ions. While, with increasing value of Gd^{3+} concentration (x = 0.01), a peak starts to appear at about ~582 eV and it has maximum value for x = 0.20. This clearly indicates that Cr^{6+} concentration increases with increasing Gd concentration. The trend of variation of activation energy, mentioned in Table 3.2, for different compositions of $La_{1-x}Gd_xCrO_3$ indicates that activation energy first decrease with x = 0.01 and thereafter it continuously increases with increasing x. This variation also supports variation of conductivity of the investigated system. The DC conductivity for the compositions $x \geq 0.10$ is found to increase very rapidly above 300 °C (in Fig.3.7). This rapid increase may be due to increase in mobility of the small polarons above this temperature. Thus above 300 °C, the conductivity in compositions $x \geq 0.10$ seems to be caused not only by the increase in number density of mobile charge carriers but also due to increase in their mobility. Nevertheless, for compositions with $x < 0.10$, above 300 °C, no considerable increase in conductivity is observed. This could be because of the oxygen vacancies, which are dominating in conduction mechanism for the compositions with $x < 0.10$, do not show any change in its mobility above 300 °C and below 520 °C [Badwal et al. (1992)].

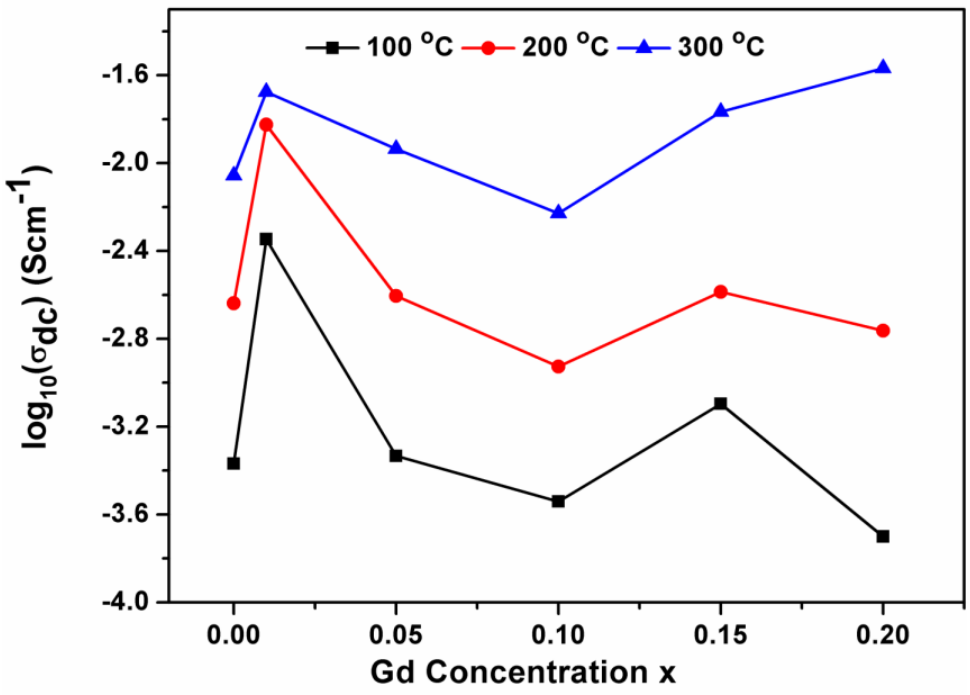

Fig. 3.7: Variation of DC conductivity with dopant concentration x in the system $La_{1-x}Gd_xCrO_3$ ($0.00 \leq x \leq 0.20$).

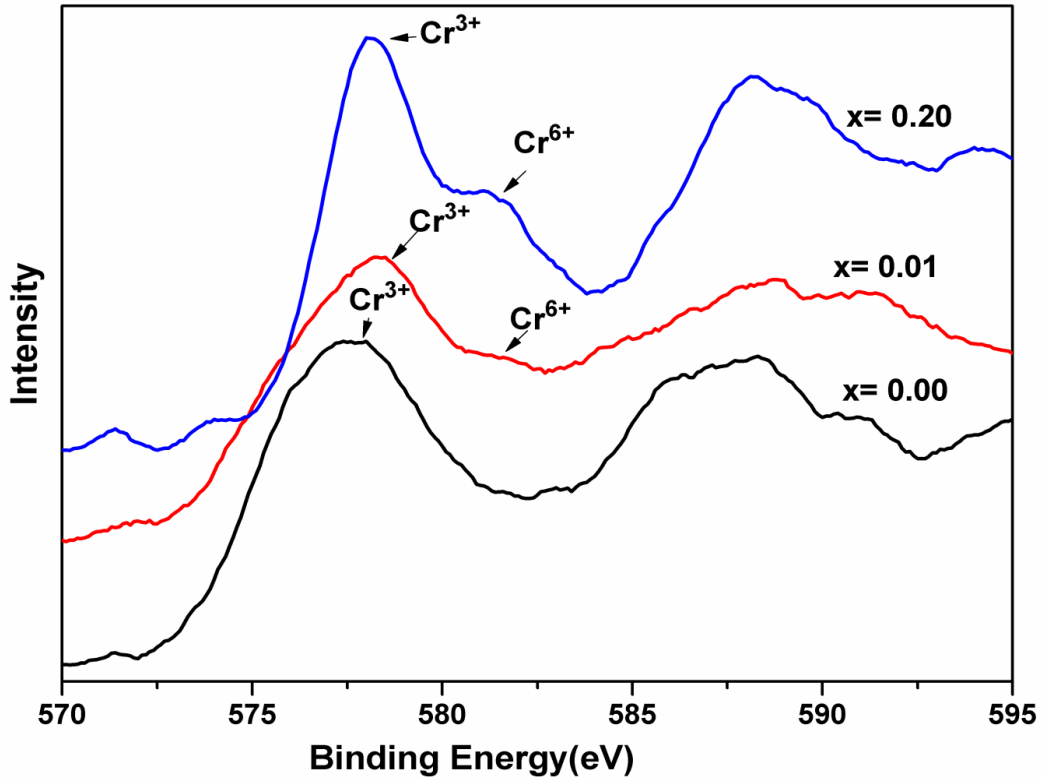

Fig. 3.8. XPS spectra of the Cr2p level in the system $La_{1-x}Gd_xCrO_3$ (x= 0.00, 0.01 and 0.20).

3.4 Conclusions

The isovalent Gd^{3+} substituted $La_{1-x}Gd_xCrO_3$ ($0.00 \leq x \leq 0.20$) nanocrystalline system is synthesized using a facile auto-combustion synthesis route. All synthesized compositions show solid solution formation having orthorhombic crystal structure similar to pure $LaCrO_3$ which is confirmed by not only in their XRD data but also in their IR spectra. The lattice parameters are found to decrease with increasing dopant concentration due to smaller size of Gd^{3+} ions in compare to La^{3+} ions. Average grain size of microscopic particles first decreases and then gradually increases with increasing dopant concentration. The DC conductivity for the compositions with $x \leq 0.01$ is found due to holes generated polarons. For compositions with $0.01 \leq x \leq 0.10$, the DC conductivity is basically governed by the oxygen ion vacancies generated due to size difference between dopant and host ions. The conductivity for compositions with $x \geq 0.10$ is mainly governed by the holes (polarons) created due to enhanced number of Cr^{6+} centres in the system. The presence of Cr^{6+} sites are confirmed in XPS measurements in $La_{1-x}Gd_xCrO_3$ system for $x > 0.00$. The compositional dependent

activation energy also supports conduction mechanism in $La_{1-x}Gd_xCrO_3$ system. Thus, this system may be proposed as a worthy system for anode materials for SOFC.